2022 International Virtual Conference on Power Engineering Computing and Control: Developments in Electric Vehicles and Energy Sector for Sustainable Future (PECCON) | 978-1-6654-8592-0/22/$31.00 ©2022 IEEE | DOI: 10.1109/PECCON55017.2022.9851032

28.81% Efficient, Low Light Intensity and High Temperature Sustainable Ultra-Thin IBC Solar Cell

Md Mahfuzur Rahman, Amirjan Bin Nawabjan
Department of Nano-Micro System Engineering, University of Technology Malaysia Johor 81310, Malaysia
Center of Electrical Energy System, Department of Nano-Micro System Engineering, University of Technology Malaysia Johor 81310
Email: mrmd4@graduate.utm.my

Abstract*— The interdigitated back contact (IBC) structure for crystalline-silicon photovoltaic device has long been recognized as an effective technique to overcome the 25% efficiency barrier by shifting all the electrical conducting elements to the backside of the cell. For this structure, the architecture of material interlayer IBC electrodes is very important to reduce the recombination rate without affecting the work function at the metal-semiconductor interface for optimum dissolution and extraction of carriers from the absorber layer. Higher efficiency requires a balance between absolute crystal material and impurities in the semiconductor, doping concentration and PN Junctions, smart grid wires and intelligent sunlight capturing. In this work, the fabrication of a low light intensity functional and high cell temperature sustainable, IBC solar cell is investigated. Silicon-Heterojunction layer to absorb greater solar spectrum and interdigitated N/P contacts have been implemented, which grants the cell to receive full surface sunlight, results in ~29% efficiency. Luminous-an optoelectronic device simulator has been utilized to construct a very thin cell with dimensions of 100x150µm. The effects of sunlight intensity and module temperature on the performance have been investigated and the parameters for the most efficient structure were found with 28.81% efficiency and 87.68% fill factor rate, making it ultra-thin, flexible and durable providing a wide range of operational capabilities.

***Keywords*— interdigitated, shading effect, recombination loss, incident-plane, drift-diffusion, Luminous, SILVACO**

I. INTRODUCTION

In typical solar cell structure connections are established at the top surface in grid pattern which produces shading loss (SL) when the covered regions of grid reflect the absorbed sunlight reducing the efficiency by 10%. Smart grid architecture generates high carrier selectivity in the absorber bulk region [1].

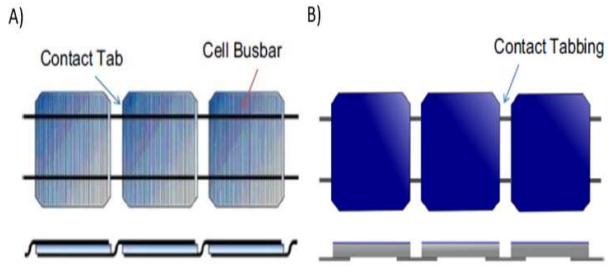

Fig. 01: (a) Conventional photovoltaic device's electrode connections on front surface (b) Structure of IBC contacts at back surface [6]

In addition, the grid electrodes possess 'grid resistance' but high conductivity is desirable for grid system to minimize resistive losses. While a relatively thick grid minimizes power dissipation, it also increases SL and narrowing contacts to avoid sunlight reflection, it increases grid resistance producing higher resistive losses [2,3]. An optimization between shading loss and resistive loss is achieved by IBC technology which shifts all contacts at the back of a photovoltaic device increasing efficiency by up to 25% where the short circuit (SC) current is higher than in conventional front surface framework solar apparatus structures [4,5].

A. Schemed IBC Architecture with Surface Texturing and Anti Reflective (AR) Metallization

In the basement, the electrodes are connected to the p and n materials in an interdigitated pattern [7]. Since the grid connections are at the back surface, it leads in a 10% increase in collected charged carriers [8] removing losses caused by the shading of the frontal grid connections on the semiconductor material [Fig. 02].

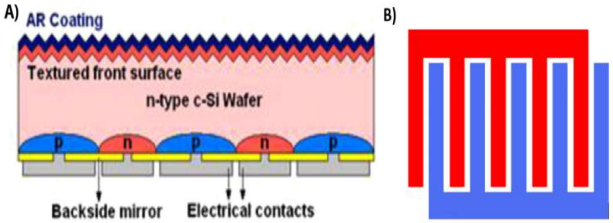

Fig. 02: (a) Designed configuration with AR coating at top and bottom interdigitated contacts (b) Interdigitated current collecting electrode pattern featuring p-type connectors in red and n-type connectors in blue [9,10]

For this designed photovoltaic device, to optimize the trapping of sunlight and to reduce the amount of reflected captured sunlight/photons, a 0.5µm thick TiO/Polysilicon (poly-Si) AR coating is applied on the top surface which is textured by utilizing 40˚ incident plane mechanism to absorb the reflected sunrays captured by the rough AR coated surface. The AR metalized coating and textured surface establish approximately 180˚ angle between the reflected sunlight and surrounding surfaces reducing the reflection by 8−10% and total reflection is reduced by less than 5% through the extended absorption of both incoming and reflected photons from sunlight [8,11].

B. Optimized Doping Concentration of PN Junction and Photon Absorbing Semiconductor Bulk

In this configuration the layer under the polysilicon pyramid structured AR metalized coating is formed by depositing SiO_2

978-1-6654-8592-0/22/$31.00 ©2022

to reduce the number of impurities in bulk. This reduces the surface recombination rate (SRV) of the silicon bulk region and reduces the recombination loss (RL) [7, 8]. The next layer is highly n+ doped to create a frontal surface field that keeps SRV ratio below $10cms^{-1}$, improving efficiency by about 28.81% for this model. The bulk region is moderately n-doped with a doping concentration in the range of $10^{10}cm^{-3}$ to $10^{15}cm^{-3}$ to generate an "extended carrier recombination time" for decrement in RL. The bulk collects the generated charged carriers or photons from sunlight. Since hole carriers move slower than electrons and they are prone to recombine before traversing the module bulk field, the p regions of the interdigitated connections are fabricated larger than the n regions resulting in a relatively limited number of hole carriers. As the carrier's path becomes faster (Fig. 02-A), the electrons flow much faster and they are less likely to recombine reducing RL producing higher SC current. The balance of the openings in these two regions (opening width 10−20 microns, Table 04-05) reduces recombination loss and provides maximum output efficiency.

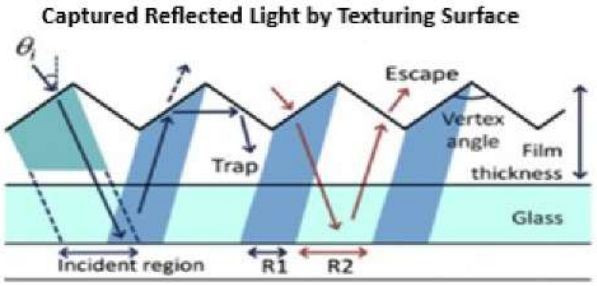

Fig. 03: Mechanism of capturing reflected sunlight and absorption of maximum sunlight implementing 40° incident plane surface texturing and AR metallization [12]

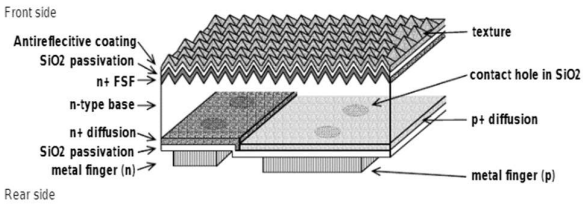

Fig. 04: SunPower corporation's A0-300 n-type silicon based solar device with metallic connections in IBC pattern [3]

For efficient output the carriers generated in the absorber must be collected and efficiently extracted at spatially separated contacts. In this structure, the passages across the n/p regions are patterned depositing SiO_2 to construct connections between the contacts and n/p regions. To reduce the RL at the interface between the aluminum mellitic contacts and the semiconductor material in bulk region, the captured sunlight is reflected back in the bulk region by the SiO_2 layer at the bottom. Fig. 04 illustrates the theoretical configuration of the described structure and mechanism.

C. Equilibrium Between Absolute Crystal and Impurities for Maximum Efficiency

Incomplete crystal structure and impurities in the semiconductor bulk region can increase the recombination loss which can be reduced by decreasing the bulk region. However, photons are less likely to generate an electron-hole pair when bulk region decreases. The electron-hole pair recombination transaction produces heat and transports it to device internal structure [8,12]. Excessive heat interferes with charge transport and causes lattice vibrations producing leakage current which reduces the efficiency [12,13]. In this structure, combinations of materials with different energy bands have been employed to form multiple junctions, which can sustain higher module temperature and enhances the performance.

II. DEVICE FABRICATION AND SIMULATION

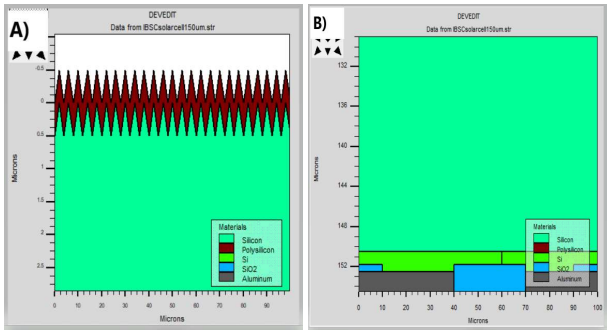

Fig. 05: (a) Top view with pyramid texturing and a metalized polysilicon AR coating (b) Bottom aluminum connector composited with SiO_2 functioning as insulator to prevent short circuit between electrodes

In this work, the photovoltaic model was fabricated using Devedit TCAD where the poly-Si anti-reflective coating and SiO_2 layer were composed initially. The pyramid-like surface texturing (red) AR metallization enhances photon absorption and the shape of this structure traps the reflected sunrays. To investigate optimum AR characteristics, Titanium Oxide (TiO) and Polysilicon were employed separately as photon parasitic layer. The next layer - front surface field is n+ doped with doping concentrations (DOPC) ranging from $10^{15}cm^{-3}$ to $10^{18}cm^{-3}$ with 0.5µm thickness, this synthesis between DOPC and thickness provides optimized open circuit voltage (V_{OC}) and short circuit current (I_{SC}) acquiring higher efficiency. The consecutive layer is bulk zone which is mildly doped n-type silicon with DOPC=$10^{15}cm^{-3}$. To generate asymmetric space charge region for efficient extraction of charge carriers the DOPC is altered from $5x10^{18}cm^{-3}$ to $5x10^{21}cm^{-3}$ at the bottom p+/n+ stripe where the p+ and n+ regions are 80µm and 20µm wide respectively maximizing output by establishing a concentration difference between electrons and holes carriers at either electrode. Finally for intelligent charge collection, microscopic aperture gaps of 10−20µm are instilled in the 1µm-SiO_2 stripe at the bottom which allows smart-interaction between IBC electrodes and n+/p+ layers.

III. RESULTS AND ANALYSIS

Atlas is a semiconductor device simulator that determines the electrical, thermal and optical characteristics of a photovoltaic apparatus implementing a combination of differential equations of Maxwell Laws and semiconductor

charge transmission. These characteristics are extracted by Atlas from physical structure of PN Junction, properties of utilized materials, DOPC, photon absorbance and bias settings [2,5-8,13,14]. In this paper, the current density is modelled using the drift-diffusion model (DDM) which is constructed by implementing approximation and simplification of three major complex equations extracted from Laws of Maxwell. The model that accounts for current produced by a photovoltaic system is developed by integrating an electron and a hole generating element to the right side of the DDM model. To solve the complete system of these equations, the Newton technique has been utilized which simulates the system until a reliable result is acquired. The following are the Maxwell and DDM equations:

$$\text{div}\,(\varepsilon\nabla\Psi) = -\rho \quad \ldots\ldots (1)$$

$$\frac{\partial n}{\partial t} = -\frac{1}{q}\text{div}\,\vec{J}_n + G_n - R_n \quad \ldots\ldots (2)$$

$$\frac{\partial p}{\partial t} = -\frac{1}{q}\text{div}\,\vec{J}_p + G_p - R_p \quad \ldots\ldots (3)$$

$$\vec{J}_n = qn\mu_n\vec{E}_n + qD_n\nabla n \quad \ldots\ldots (4)$$

$$\vec{J}_p = qp\mu_p\vec{E}_p - qD_p\nabla p \quad \ldots\ldots (5)$$

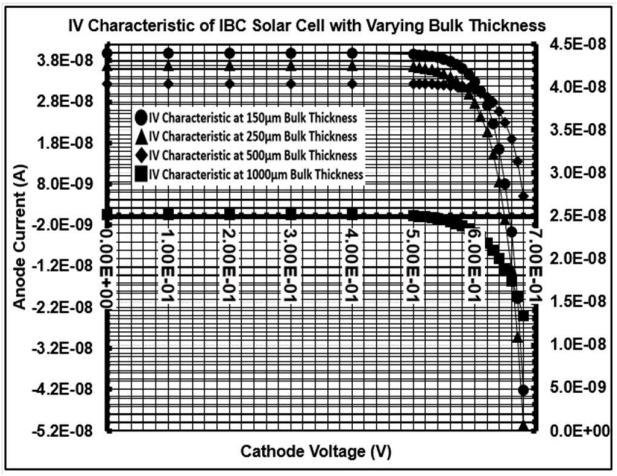

Fig. 06: IV characteristic with varying bulk thickness

A. *Device Effectiveness Depending on The Thickness of The Bulk Region*

Fig. 06 characterizes the IV curve of 100x150µm, 100x250µm, 100x500µm and 100x1000µm designed photovoltaic devices. As shown in the data (Table-01), the I_{SC} accelerating in proportion to bulk thickness because for photocurrent generation, the bulk portion gathers photons from sunlight and if the bulk zone is too narrow the excited charge carriers will have very limited time to transverse the cell area (diffusion distance - DFSD) resulting in a higher RL. But when the bulk region increases, it absorbs more photons, additionally DFSD rises and RL declines leading to a greater I_{SC}. Table-01 reports the impact of bulk thickness. For the 100x100µm diameter device the graph (Fig. 06) indicates V_{OC}=0.680V and Isc=0.04038µA. Although the 100x1000µm cell does have a strong I_{SC}, it is not versatile or suitable to modern applications that demand ultra-thin and flexibility.

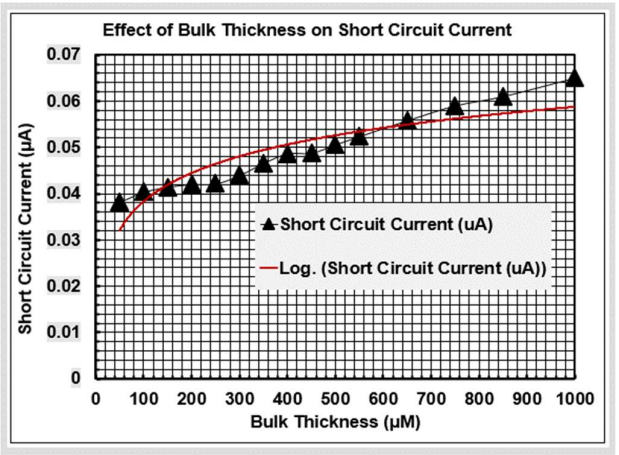

Fig. 07: Analyzation of the stability of I_{SC} assisted by the graphical interrelation between I_{SC} and bulk region width

The I_{SC} dropped by about 0.01444µA after a 500µm reduction in bulk region. Flexible photovoltaic devices are those with a bulk thickness of less than 200µm [15]. A large I_{SC} of 0.04147µA is produced by the designed ultra-thin 100x150µm device. Fig. 07 depicts Dependency of I_{SC} on varying bulk thickness.

Table 01: Dependency of I_{SC} on Varying Bulk Thickness

Bulk Width (µm)	Module Temperature (K)	Light Intensity (watt/cm^2)	VOC (V)	ISC (µA)
100	298	1.00	0.68	0.04038
150	298	1.00	0.68	0.04147
250	298	1.00	0.68	0.04218
500	298	1.00	0.68	0.05063
650	298	1.00	0.68	0.05587
750	298	1.00	0.68	0.05908
850	298	1.00	0.68	0.06109
1000	298	1.00	0.68	0.06507

B. *Investigation of Low Light Intensity on The Developed Photovoltaic Technology*

To evaluate the influence of light intensity the Luminous Tool is employed which determines the light propagation and absorption rates for photocurrent generation by computing the optical intensity within a photovoltaic surface. Luminous is also able to generate the AR metalized coating which has been utilized in this design. To investigate the performance in low light intensity, gradual changes have been made in light beam intensity (LBI) and the findings (Table-02) show that I_{SC} is proportional to LBI and the developed design is exceedingly light adapted which generates significant I_{SC} at low light ambient.

Table 02: Effect of Light Intensity on The Designed IBC Solar System

Bulk Thickness (µm)	Temperature (K)	Light Intensity (watt/cm^2)	VOC (V)	ISC (µA)	ISC (µA)
				Poly- Si AR Coating	TiO AR Coating
250	298	0.00	0.68	0.03807	0.29952

250	298	0.10	0.68	0.03879	0.32581
250	298	0.30	0.68	0.03956	0.35678
250	298	0.50	0.68	0.03998	0.45176
250	298	0.70	0.68	0.04052	0.47152
250	298	1	0.68	0.04218	0.95789

According to the preceding statistics and graphical view (Fig. 08), the I_{SC} is 0.03879μA at a LBI of 0.1watt/cm^2. From 0watt/cm^2–1watt/cm^2 LBI, I_{SC} is quite steady. In addition, at 0watt/cm^2 LBI, the I_{SC} is 0.03807μA, indicating that even on average days when the sunlight is not particularly high, the designed photovoltaic IBC technology still delivers outstanding output. These responses of the device demonstrates that the proposed device works effectively in low-light conditions. The study also revealed that TiO coating is superior to polysilicon coating because TiO minimizes sunlight reflection more efficiently than polysilicon, resulting in a higher I_{SC}. However, the poly-Si anti reflective coating configuration has been carried out in this study in compliance with conventional AR practice.

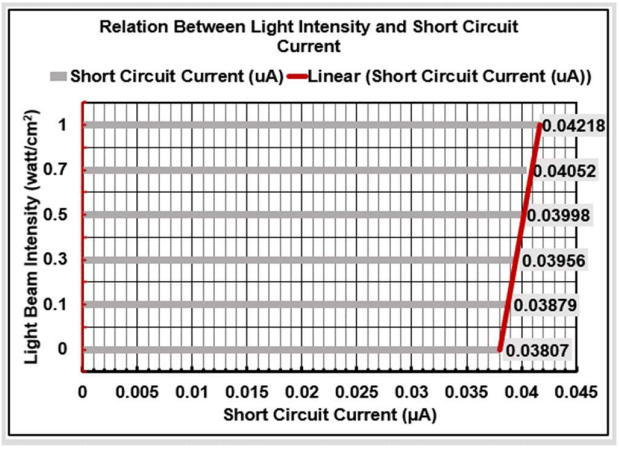

Fig. 08: The dependency between incident LBI and I_{SC} in graphical form

C. *Inspection of Temperature Effect on the IBC Photovoltaic Structure (150m Bulk Thickness)*

Since photovoltaic devices are comprised of semiconductors, these are temperature sensitive. To study the influence of temperature, simulations were conducted on the 'identical device' at temperatures ranging from 0˚C to 50˚C implementing single wavelength light of 10watt/cm^2. Rise in temperature alters properties of semiconductor because bandgap (eV) of a semiconductor material expands with temperature, accelerating the energy of the electrons in the bulk region causing the electron-hole pair bonds to be broken with less energy. During this period, thermal ionization occurs instigating electrons and holes split generating leakage current that flows in opposite direction of photocurrent reducing overall I_{SC} [13,16,17]. The leakage current rises with modulate temperature due to this electron-hole split conjuncture. The temperature effect in a photovoltaic device can be explained implementing the following equation of comprised current density:

$$J(I,V) = J_d(V) + J_{sh}(V) - J_{ph}(I,V) \ldots\ldots\ldots\ldots (6)$$

where, Jd = diode current density, Jph = photocurrent density and Jsh = leakage current density

In a solar appliance, leakage current injected from the electrodes prior to the turn on voltage (0V to V_{OC}), flows in the opposite direction of photocurrent and reduces the total I_{SC} [18]. The data in Table-03 depicts the effect of temperature on the performance of the designed structure. The 'preferred temperature'−25˚C to test photovoltaic performance has also been reported.

Table 03: Effect of Module Temperature on I_{SC} (V_{OC} = 0.680V)

Bulk (μm)	V_{OC} (V)	Module Temperature		LBI (watt/cm^2)	I_{SC} (μA)
250.0	0.68	273.0K	0.0ºC	10.0	0.39724
250.0	0.68	288.0K	15.0ºC	10.0	0.38779
250.0	0.68	293.0K	20.0ºC	10.0	0.38756
250.0	0.68	298.0K	25.0ºC	10.0	0.38733
250.0	0.68	303.0K	30.0ºC	10.0	0.38709
250.0	0.68	308.0K	35.0ºC	10.0	0.38686
250.0	0.68	323.0K	50.0ºC	10.0	0.38618

From the analysis of the relationship between the simulated data in Table-03 and the graph (Fig. 09), we can conclude that the constructed IBC cell operates extremely well enough at 0˚C. The IV curve, on the other hand, declines infinitesimally as the temperature rises. The IV curve reveals that the cell offers I_{SC} of 0.38618μA from 288K (15˚C) to 323K (50˚C) with a minor decline in I_{SC} and at 298K (25˚C) the system provides I_{SC} of 0.38733μA. These parameters reveal that the developed device functions very efficiently even at high module temperatures which is a key measurement for solar device output proving that the system can withstand temperature of up to 50˚C.

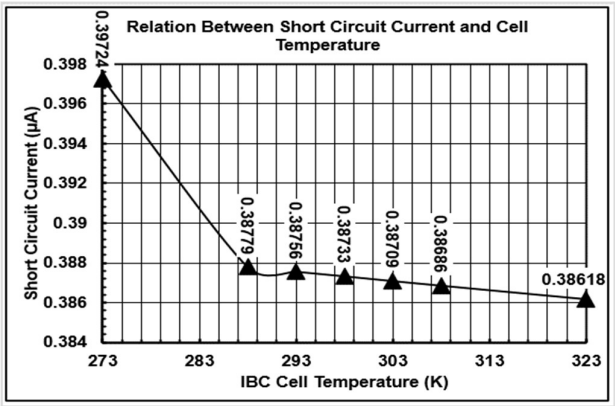

Fig. 09: Module temperature and SC current correlation

D. *Assessment of Fill Factor and Efficiency*

There are several elements considered while assessing the photovoltaic performance. The V_{OC} and I_{SC} are the two variables that represent the maximum voltage and output current respectively and used as performance indicators. The fill factor (FF) is a stronger predictor which is the measurement of how closely a photovoltaic device performs to an ideal source. The standard value of FF is around 80% [19]. Efficiency is the most accurate parameter since it relates

the input and output power and a better solar cell is one with higher efficiency. Therefore, the analytical findings in Table-04, which include FF and efficiency, reflect the overall performance evaluation of the device.

Table 04: Synopsis of Efficiency and Output Readability (Photovoltaic Active Sphere = 100cm^2, Module Thermal Condition = 25ºC and LBI = 1watt/cm^2)

Bulk Width (µm)	V_{OC} (V)	I_{SC} (µA)	Maximum Power (mW)	Short circuit current density (mA/cm^2)	Fill Factor, FF (%)	Efficiency (%)
50.0	***0.68***	***0.03821***	***0.02098***	***38.1954***	***80.105***	***25.067***
150.0	***0.68***	***0.04147***	***0.02182***	***40.3783***	***79.407***	***26.078***
250.0	***0.68***	***0.04218***	***0.02117***	***42.1719***	***73.778***	***25.297***
400.0	0.68	0.04872	0.01994	48.6977	60.196	23.833
500.0	0.68	0.05065	0.19167	50.6244	55.676	22.914
650.0	0.68	0.05588	0.01791	55.8572	47.054	21.377
750.0	0.68	0.05908	0.01705	59.0542	42.398	20.355
850.0	0.68	0.06109	0.01627	60.8503	39.207	19.406
1000.0	0.68	0.06508	0.01504	65.0608	33.885	17.927

The optimum performance of the designed photovoltaic apparatus is investigated in Table 05 by altering the module thermal state to 15˚C, because this is the temperature at which a solar system maintains its peak efficiency [16].

Table 05: Synopsis of Efficiency and Output Readability (Photovoltaic Active Sphere = 100cm^2, Module Thermal Condition = 15ºC and LBI = 1watt/cm^2)

Bulk Thickness (µm)	V_{OC} (V)	ISC (µA)	Maximum Power (mW)	Short circuit current density (mA/cm^2)	Fill Factor, FF (%)	Efficiency (%)
50.0	***0.68***	***0.03827***	***0.02314***	***38.2019***	***88.975***	***27.649***
150.0	***0.68***	***0.04173***	***0.02415***	***40.4055***	***87.688***	***28.817***
250.0	***0.68***	***0.04306***	***0.02347***	***43.1516***	***86.637***	***28.048***
400.0	0.68	0.04903	0.02224	49.1250	85.445	26.565
500.0	0.68	0.05105	0.02142	51.9549	84.867	25.554

Table 06: Comparison of Device Performance with Recently Designed Interdigitated Back Contact Solar Devices

Paper/Parameters	Morris Dahlinger et al [22], 2013	Hao Lin et al [24], 2018	Weiliang Wu et al [2] 2018	Nadjat Benadla et al [20], 2019	S. Schäfera et al [21], 2019	Proposed Cell
Open circuit voltage (mV)	669	590	709	635	700	680
Short circuit current density (mA/cm^2)	41.30	30.2	41.50	39.20	42.50	40.40
Fill Factor, FF (%)	79.80	72.6	75.60	77.70	80.70	87.68
Efficiency (%)	22.20	12.5	22.20	20.19	26.00	28.81

Based on the reported findings in Table-05, it can be determined that the IBC photovoltaic device with a dimension of 100x150µm has the highest efficiency of 28.817% and an FF of 87.688%. Another striking observation is the correlation between bulk thickness and efficiency where the I_{SC} grows in proportion to bulk region width because the surface absorbs more incident LBI. In addition, photons decay exponentially with the distance traveled in bulk region increasing electron-hole pairs and photocurrent. When the travelling distance exceeds the average length that a charge carrier moves between generation and recombination period, the sheet resistance decreases, resulting in a greater FF, although this phenomenon reduces efficiency [22,23]. As a result, selecting the appropriate bulk thickness is an important and crucial step for back-contact solar apparatus. Having accomplished a balancing optimization between bulk thickness and maximum efficiency in this research, the results shows that 100x50µm to 100x250µm dimensioned cells yield extremely promising outcomes. The device with a bulk thickness of 50µm has an optimal efficiency of 27.649% and an FF of 88.975%, retains ultra-thin photovoltaic device fabrication while establishing excellent device performance.

E. Evaluation of the Engineered Technology in Perspective of Recent IBC Works

This section compares the performance of proposed device to that of comparable IBC solar appliances recently constructed by other researchers considering the four main parameters of a photovoltaic device analyzers: V_{OC}, SC current density (JSC), FF and efficiency. The optimal performance for each device has been taken into account in this analysis (Table-06).

IV. CONCLUSION

In this research, *SILVACO TCAD* was implemented to construct an interdigitated back-contact photovoltaic device with a 100cm^2 active surface area based on the SunPower A-300 configuration. The simulated design was subjected to a series of parameter changes in order to assess its performance. The influence of bulk thickness and silicon-heterojunction layer on efficiency have been investigated and the results reveal that as bulk thickness grows, it collects more photons which increase the I_{SC}, but efficiency drops due to

recombination loss and diffusion length. The devices with dimensions of 100x50µm, 100x150µm and 100x250µm achieved a maximum efficiency of 27.64%–28.81% with an outstanding Fill Factor of around 87%–89% indicating that ultra-thin solar cells can provide effective output. Luminous tool was used to test the effect of low light intensity with 0,0.1,0.3,0.5,0.7 and 1watt/cm^2 and the findings suggest that the system operates satisfactorily even on a typical day at low light intensity of 1watt/cm^2. The studies also suggest that when the light intensity increases, the I_{SC} increases significantly, implying a highly light efficient solar technology. The final inspection of the module temperature shows that as the temperature rises from 0˚C to about 15˚C, the I_{SC} drops by 0.009µA, but after 15˚C, the I_{SC} persists despite any change in thermal reading demonstrating that the developed technology is a promising temperature adequate photovoltaic device that retains its functionality even up to 50˚C.

REFERENCES

[1]. C. Hollemann et al., "Separating the two polarities of the POLO contacts of an 26.1%-efficient IBC solar cell", Scientific Reports, vol. 10, no. 1, 2020. Available: 10.1038/s41598-019-57310-0

[2]. W. Wu et al., "22% efficient dopant-free interdigitated back contact silicon solar cells", 2018. Available: 10.1063/1.5049288.

[3]. D. Song et al., "Progress in n-type Si solar cell and module technology for high efficiency and low cost", 2012 38th IEEE Photovoltaic Specialists Conference, 2012. Available: 10.1109/pvsc.2012.6318216

[4]. C. Hollemann, F. Haase, S. Schäfer, J. Krügener, R. Brendel and R. Peibst, "26.1%-efficient POLO-IBC cells: Quantification of electrical and optical loss mechanisms", Progress in Photovoltaics: Research and Applications, vol. 27, no. 11, pp. 950-958, 2019. Available: 10.1002/pip.3098

[5]. E. Bellini, "Novel IBC solar cell architecture based on crystal photonics shows efficiency potential of 29.1%", pv magazine International, 2022. [Online]. Available: https://www.pv-magazine.com/2022/02/18/novel-ibc-solar-cell-architecture-based-on-crystal-photonics-shows-efficiency-potential-of-29-1/

[6]. M. Mat Desa et al., "Silicon back contact solar cell configuration: A pathway towards higher efficiency", Renewable and Sustainable Energy Reviews, vol. 60, pp. 1516-1532, 2016. Available: 10.1016/j.rser.2016.03.004

[7]. M. Kim, J. Lee and M. Kwak, "Review: Surface Texturing Methods for Solar Cell Efficiency Enhancement", International Journal of Precision Engineering and Manufacturing, vol. 21, no. 7, pp. 1389-1398, 2020. Available: 10.1007/s12541-020-00337-5.

[8]. R. Jeyakumar et al., "High-efficiency c-Si based interdigitated point contact back heterojunction solar cells", Journal of Materials Science: Materials in Electronics, vol. 28, no. 13, pp. 9697-9703, 2017. Available: 10.1007/s10854-017-6720-1

[9]. Mat Desa, M., Sapeai, S., Azhari, A., Sopian, K., Sulaiman, M., Amin, N. and Zaidi, S., 2016. Silicon back contact solar cell configuration: A pathway towards higher efficiency. Renewable and Sustainable Energy Reviews, 60, pp.1516-1532.

[10]. N. Guerra, M. Guevara, C. Palacios and F. Crupi, "Operation and physics of photovoltaic solar cells: an overview", I+D Tecnológico, vol. 14, no. 2, pp. 84-95, 2018. Available: 10.33412/idt.v14.2.2077.

[11]. T. M. Letcher and V. M. Fthenakis, "Photovoltaics: The Basics. A Comprehensive Guide to Solar Energy Systems", 2018.

[12]. S. Iftiquar and J. Yi, "Numerical simulation and light trapping in perovskite solar cell", Journal of Photonics for Energy, vol. 6, no. 2, p. 025507, 2016. Available: 10.1117/1.jpe.6.025507.

[13]. C. Battaglia, A. Cuevas and S. De Wolf, "High-efficiency crystalline silicon solar cells: status and perspectives", Energy & Environmental Science, vol. 9, no. 5, pp. 1552-1576, 2016. Available: 10.1039/c5ee03380b

[14]. "Atlas User Manual Device Simulation Software", SILVACO® (2016) ATLAS™, 2016. [Online]. Available: https://dynamic.silvaco.com/dynamicweb/jsp/downloads/DownloadManualsAction.do?req=silen-manuals&nm=atlas

[15]. H. Um, I. Hwang, D. Choi and K. Seo, "Flexible Crystalline-Silicon Photovoltaics: Light Management with Surface Structures", Accounts of Materials Research, vol. 2, no. 9, pp. 701-713, 2021.

[16]. Honsberg, C. and Bowden, S., 2021. Effect of Temperature | PVEducation. Pveducation.org. Available at: https://www.pveducation.org/pvcdrom/solar-cell-operation/effect-of-temperature.

[17]. A. Routray and S. Hur, "Leakage Current Mitigation of Photovoltaic System Using Optimized Predictive Control for Improved Efficiency", Applied Sciences, vol. 12, no. 2, p. 643, 2022. Available: 10.3390/app12020643

[18]. C. Proctor and T. Nguyen, "Effect of leakage current and shunt resistance on the light intensity dependence of organic solar cells", Applied Physics Letters, vol. 106, no. 8, p. 083301, 2015. Available: 10.1063/1.4913589

[19]. M. Dar and S. Ahmed, "Effect of light and heavy ion irradiation on graphene device matrix: Optical and Transport Characteristics", Radiation Physics and Chemistry, vol. 156, pp. 67-72, 2019. Available: 10.1016/j.radphyschem.2018.09.027.

[20]. N. Benadla and K. Ghaffour, "Optimizing the performance of photovoltaic cells IBC (contact back interdigitated) by numerical simulation", International Journal of Electrical and Computer Engineering (IJECE), vol. 9, no. 6, p. 4566, 2019. Available: 10.11591/ijece.v9i6.pp4566-4572.

[21]. Schäfer, S., Haase, F., Hollemann, C., Hensen, J., Krügener, J., Brendel, R. and Peibst, R., 2019. 26%-efficient and 2 cm narrow interdigitated back contact silicon solar cells with passivated slits on two edges. Solar Energy Materials and Solar Cells, 200, p.110021.

[22]. M. Dahlinger, B. Bazer-Bachi, T. Röder, J. Köhler, R. Zapf-Gottwick and J. Werner, "22.0% Efficient Laser Doped back Contact Solar Cells", Energy Procedia, vol. 38, pp. 250-253, 2013. Available: 10.1016/j.egypro.2013.07.274.

[23]. A. Abdelnaby Zekry, "Advanced solar cell materials and solar cells analytical modeling", 2017. Available: 10.13140/RG.2.2.26299.31527.

[24]. H. Lin et al., "Realization of interdigitated back contact silicon solar cells by using dopant-free heterocontacts for both polarities", Nano Energy, vol. 50, pp. 777-784, 2018. Available: 10.1016/j.nanoen.2018.06.013